

Article

# Impact of TiO<sub>2</sub> Reduction and Cu Doping on Bacteria Inactivation under Artificial Solar Light Irradiation

Piotr Rychtowski <sup>1,\*</sup>, Oliwia Paszkiewicz <sup>2</sup>, Maria Carmen Román-Martínez <sup>3</sup>,  
 Maria Ángeles Lillo-Ródenas <sup>3</sup>, Agata Markowska-Szczupak <sup>2</sup> and Beata Tryba <sup>1</sup>

- <sup>1</sup> Department of Catalytic and Sorbent Materials Engineering, Faculty of Chemical Technology and Engineering, West Pomeranian University of Technology in Szczecin, Pułaskiego 10, 70–322 Szczecin, Poland
- <sup>2</sup> Department of Chemical and Process Engineering, West Pomeranian University of Technology, Piastów 42, 71–065 Szczecin, Poland
- <sup>3</sup> Department of Inorganic Chemistry and Materials Institute (IUMA), Faculty of Sciences, University of Alicante, Carretera de San Vicente del Raspeig s/n, 03690 Alicante, Spain
- \* Correspondence: piotr.rychtowski@zut.edu.pl

**Abstract:** Preparation of TiO<sub>2</sub> using the hydrothermal treatment in NH<sub>4</sub>OH solution and subsequent thermal heating at 500–700 °C in Ar was performed in order to introduce some titania surface defects. The highest amount of oxygen vacancies and Ti<sup>3+</sup> surface defects were observed for a sample heat-treated at 500 °C. The presence of these surface defects enhanced photocatalytic properties of titania towards the deactivation of two bacteria species, *E. coli* and *S. epidermidis*, under artificial solar lamp irradiation. Further modification of TiO<sub>2</sub> was targeted towards the doping of Cu species. Cu doping was realized through the impregnation of the titania surface by Cu species supplied from various copper salts in an aqueous solution and the subsequent heating at 500 °C in Ar. The following precursors were used as a source of Cu: CuSO<sub>4</sub>, CuNO<sub>3</sub> or Cu(CH<sub>3</sub>COO)<sub>2</sub>. Cu doping was performed for raw TiO<sub>2</sub> after a hydrothermal process with and without NH<sub>4</sub>OH addition. The obtained results indicate that Cu species were deposited on the titania surface defects in the case of reduced TiO<sub>2</sub>, but on the TiO<sub>2</sub> without NH<sub>4</sub>OH modification, Cu species were attached through the titania adsorbed hydroxyl groups. Cu doping on TiO<sub>2</sub> increased the absorption of light in the visible range. Rapid inactivation of *E. coli* within 30 min was obtained for the ammonia-reduced TiO<sub>2</sub> heated at 500 °C and TiO<sub>2</sub> doped with Cu from CuSO<sub>4</sub> solution. Photocatalytic deactivation of *S. epidermidis* was greatly enhanced through Cu doping on TiO<sub>2</sub>. Impregnation of TiO<sub>2</sub> with CuSO<sub>4</sub> was the most effective for inactivation of both *E. coli* and *S. epidermidis*.

**Keywords:** photocatalysis; reduced TiO<sub>2</sub>; Cu-TiO<sub>2</sub>; solar lamp irradiation; *E. coli*; *S. epidermidis*



**Citation:** Rychtowski, P.; Paszkiewicz, O.; Román-Martínez, M.C.; Lillo-Ródenas, M.Á.; Markowska-Szczupak, A.; Tryba, B. Impact of TiO<sub>2</sub> Reduction and Cu Doping on Bacteria Inactivation under Artificial Solar Light Irradiation. *Molecules* **2022**, *27*, 9032. <https://doi.org/10.3390/molecules27249032>

Academic Editor: Sergio Navalon

Received: 22 November 2022

Accepted: 15 December 2022

Published: 18 December 2022

**Publisher's Note:** MDPI stays neutral with regard to jurisdictional claims in published maps and institutional affiliations.



**Copyright:** © 2022 by the authors. Licensee MDPI, Basel, Switzerland. This article is an open access article distributed under the terms and conditions of the Creative Commons Attribution (CC BY) license (<https://creativecommons.org/licenses/by/4.0/>).

## 1. Introduction

Among all photocatalysts, TiO<sub>2</sub>-based materials are the most popular due to their low cost, great stability, ease of metal doping and relatively high activity [1]. However, due to their wide band gap value, many attempts have been made to increase their light harvesting in the visible range. In addition, the bacteria inactivation mechanisms, particularly in the case of copper-modified titanium dioxide, the mechanism is still unclear and some reports indicate a synergistic antibacterial effect of Cu and photocatalytically active TiO<sub>2</sub> [2]. Nevertheless, there is a need to boost TiO<sub>2</sub>-based materials' activity.

Most popular modification methods among scientists are based upon the utilization of noble (Pt, Au, Ag) or transition metals (Fe, Cu), as well as the non-metal dopants such as S, F, N and C [3–6]. One of the most exceptional modification approaches is the creation of Ti<sup>3+</sup> surface defects on TiO<sub>2</sub>, which not only increase visible light utilization, but also boost the separation of electron–hole pairs, leading to the improved formation of reactive radicals [7–11]. Ti<sup>3+</sup> self-doping appears to be an effective way of boosting TiO<sub>2</sub> antimicrobial activity in the visible

range [11], whereas some reports [12] have indicated successful utilization of antimicrobial properties of  $Ti^{3+}$  /Cu-modified  $TiO_2$  composites.

The bacteriostatic properties of copper compounds have been known for decades due to their toxicity towards pathogenic bacteria [13]. According to some reports [14], noble and semi-noble metal dopants increase the possibility of radical formation. The increase in activity is as follows:  $TiO_2$ -Cu >  $TiO_2$ -Au >  $TiO_2$ -Ag >  $TiO_2$ . However, photocatalytic inactivation of bacteria is more complex and not only focuses on reactive radical formation. For example, the photocatalytic inactivation of Gram-negative *Escherichia coli* using nanomaterials based on Cu-doped  $TiO_2$  proves to be an effective method, because it connects antibacterial properties of Cu and photocatalytic properties of  $TiO_2$ , as well as facilitates charge transfer due to efficient heterojunction between both semi-conductors [2,15,16].

The most popular methods of obtaining  $TiO_2$ -Cu composites are by using sol-gel [17,18], wet impregnation [19], magnetron sputtering [15] and thin films formation [20].

Cu-doped  $TiO_2$  preparation through the sol-gel method [18] showed the best results in the photocatalytic inactivation of Gram-negative bacteria *E. coli* under visible light, where 3% of Cu was introduced. It is worth mentioning that Cu doping of  $TiO_2$  led to improved visible light activity as well as improved stability of electron-hole pairs, followed by an increased reactive radical life-time. In the case of Gram-positive bacteria *Staphylococcus aureus*, the utilization of  $TiO_2$ -Cu nanomaterials [21] showed long-term antibacterial properties and prevented secondary bacterial infections of orthopedics implants.

Wet-impregnated  $TiO_2$  with Cu salts, where 0.5 M% of copper was introduced to  $TiO_2$ , appears to be an effective preparation method for obtaining effective photocatalysts for the disinfection of *E. coli* in river water [19]. However, the authors suggest that its high efficiency might be connected to the diffusion of Cu ions out of the titania matrix into the bacteria solution, meaning that the sample prepared in this way is most likely unstable and single-use. In order to obtain a reusable and stable photocatalyst, a preparation method in which Cu ions will be preserved in  $TiO_2$  matrix is required. Another important aspect is the loading of Cu-based dopants. A high percentage of copper dopants resulted in a great decrease of the specific surface area of  $TiO_2$ , which lowers the adsorption of bacteria on reactive sites [19]. On the other hand, pH value, which directly affects PZC (point zero charge), also has a great effect on *E. coli* adsorption, leading to better photocatalytic deactivation efficiency in shorter time periods. Taking electrostatic forces into account, a lower pH value than PZC might be favored for *E. coli* adsorption. Bearing this in mind, the utilization of different Cu-based dopants will result in varied forces that will either attract bacteria into the photocatalyst porous surface or push them away.

T. Lopez and others [14] performed an in-depth XPS analysis of Cu/ $TiO_2$  materials. They came to the conclusion that the most promising results of *E. coli* DNA degradation are obtained when  $Cu^{1+}$  and  $Ti^{3+}$  species are present in the crystal lattice of studied composites. It is therefore important as to which oxidation state of copper the Cu/ $TiO_2$  composite consists of. In our previous works [8–10], we introduced efficient methods of  $Ti^{3+}$  formation on the surface of  $TiO_2$ .

In this research article, we compared different  $TiO_2$  modification methods using reductive environment (aqueous  $NH_3$ , gaseous  $NH_3$  or  $H_2$ ) versus modification with Cu-based dopants ( $Cu(NO_3)_2$ ,  $CuSO_4$  or  $Cu(CH_3COO)_2$ ), where Cu load was 1.0 wt%. All preparations were performed via high-temperature calcination. Both groups of samples were utilized in the photocatalytic deactivation of model bacteria: *Escherichia coli* (Gram-negative) and *Staphylococcus epidermidis* (Gram-positive) in the presence of artificial solar light.

## 2. Results

### 2.1. X-ray Diffraction and TEM Analyses

X-ray diffractograms are presented in Figure 1. The increase in heat-treatment temperature led to an increase in the crystallinity of the anatase, as observed by the appearance of narrower and more intense reflexes. The ratio of anatase to rutile was around 96/4, respectively, and was maintained among all of the prepared samples with the exception

of TiO<sub>2</sub> heat-treated at 700 °C after NH<sub>4</sub>OH modification, which was composed from mixed phases, anatase and rutile with a ratio of 55/45, respectively. Modification of TiO<sub>2</sub> with NH<sub>4</sub>OH accelerated its crystallization and phase transformation to rutile. In Table 1, calculated crystallite sizes for all of the studied samples based on the Scherrer equation are listed.

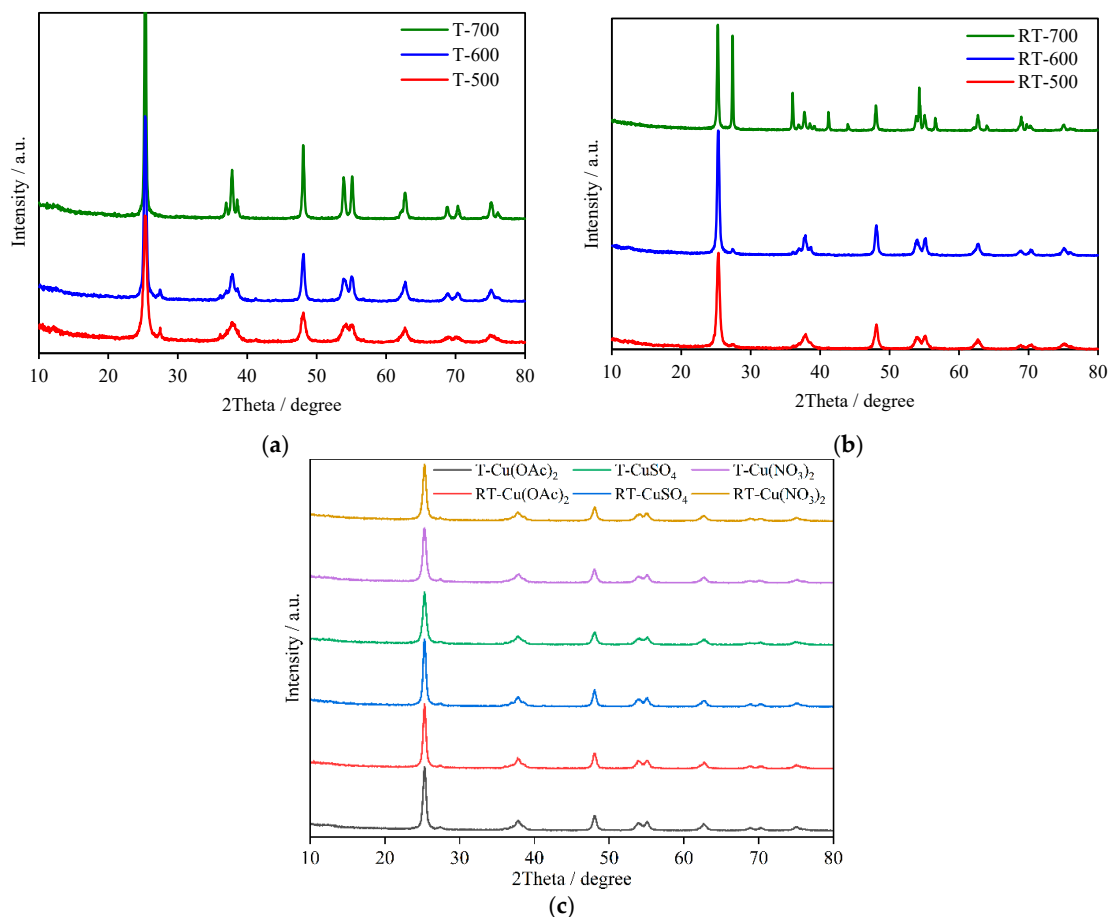


**Figure 1.** XRD diffractograms of (a) TiO<sub>2</sub> obtained in hydrothermal process and heat-treated at 500–700 °C, (b) TiO<sub>2</sub> obtained in hydrothermal process with NH<sub>4</sub>OH and heat-treated at 500–700 °C, (c) Cu-TiO<sub>2</sub> samples.

**Table 1.** Mean crystallite size of anatase and rutile in TiO<sub>2</sub> determined from the Scherrer equation (using XRD analyses).

Sample	Mean Crystallite Size/nm	
	Anatase	Rutile
Raw TiO <sub>2</sub>	12	19
T-500	17	70
T-600	26	51
T-700	48	–
RT-500	21	24
RT-600	30	37
RT-700	56	177
T-Cu(OAc) <sub>2</sub>	20	14
RT-Cu(OAc) <sub>2</sub>	22	23
T-CuSO <sub>4</sub>	16	16
RT-CuSO <sub>4</sub>	23	16
T-Cu(NO <sub>3</sub> ) <sub>2</sub>	18	20
RT-Cu(NO <sub>3</sub> ) <sub>2</sub>	19	26

The structural appearance of TiO<sub>2</sub> samples and Cu nanoparticles' presence were measured via the TEM method (Figures S1–S7 in the Supplementary Materials). Both of the crystallites of anatase and rutile were visible and their size was varied from a few to over 20 nm. The nanoparticles of copper were also observed; however, their amount was low due to their low concentration in samples and very low size.

## 2.2. X-ray Fluorescence Spectroscopy

In Table 2, the resulting data from XRF measurements are presented. The raw TiO<sub>2</sub> contained around 1.5 mass% of sulfur, because this material was a semi-product from the industrial production of titania white. TiO<sub>2</sub> samples modified with NH<sub>4</sub>OH contained a lower quantity of sulfur in comparison with those which were prepared without the pretreatment of TiO<sub>2</sub> with ammonia solution. Most likely, ammonia species rinsed some of the sulfate groups from the titania surface. Amounts of Cu in all the Cu-doped TiO<sub>2</sub> samples were comparable.

**Table 2.** XRF analysis: mass content of titanium (Ti), copper (Cu) and sulfur (S).

Sample	XRF Mass Content/%		
	Ti	Cu	S
Raw TiO <sub>2</sub>	84.26	–	1.54
T-Cu(OAc) <sub>2</sub>	77.63	1.65	0.72
RT-Cu(OAc) <sub>2</sub>	80.70	1.62	0.11
T-CuSO <sub>4</sub>	77.38	1.60	1.52
RT-CuSO <sub>4</sub>	81.42	1.59	0.40
T-Cu(NO <sub>3</sub> ) <sub>2</sub>	77.16	1.67	1.24
RT-Cu(NO <sub>3</sub> ) <sub>2</sub>	80.66	1.50	0.14

## 2.3. Fourier-Transform Infrared Spectroscopy (FTIR)

In Figure 2a–d, FTIR spectra of prepared samples are presented.

In all the FTIR spectra there is a characteristic band at 1630–1620 cm<sup>−1</sup> corresponding to the stretching vibrations of hydroxyl groups in TiO<sub>2</sub> [22]. Some sulfur surface groups were identified in some of the titania samples, with a wide band at around 1240 cm<sup>−1</sup> [23]. The presence of sulfur species resulted from the origin of a raw titania, which was supplied by the chemical factory (Grupa Azoty S.A. Police, Poland). A noticeable decrease in the band intensity at around 1240 cm<sup>−1</sup> was observed for the titania samples reduced with NH<sub>4</sub>OH (Figure 2a). Most likely, some of the ammonia species such as NH<sub>4</sub><sup>+</sup> ions could adsorb on the sulfated titania to form ammonia sulfate, which was then removed from the surface during further treatment. However, modification of titania with CuSO<sub>4</sub> (Figure 2c) caused an increase in the intensity of this band due to the naturally bounded SO<sub>4</sub><sup>2−</sup> species during the wet-impregnation process. Preparation of the TiO<sub>2</sub> with NH<sub>4</sub>OH modification caused some changes in its chemical structure; two new bands were formed, at around 1440 and 1545 cm<sup>−1</sup>, which could be assigned to the NO<sub>2</sub> stretching vibrations: symmetric and asymmetric, respectively [10]. These bands were formed upon decomposition of earlier-adsorbed ammonia groups, through the interaction of nitrogen with oxygen built in the titania lattice. A mechanism of NO<sub>2</sub> formation on TiO<sub>2</sub> modified by an ammonia species was described elsewhere [10]. The impregnation of TiO<sub>2</sub> with Cu(OAc)<sub>2</sub> (Figure 2b) caused the appearance of a new small-intensity band at the range of 1500–1400 cm<sup>−1</sup>, which could be assigned to some COO groups [22]. Additionally, Cu(OAc)<sub>2</sub> adsorbed on the reduced titania exhibited a band at around 1620 cm<sup>−1</sup> with two humps, from the left and right sides. Most likely, some of the acetate groups were adsorbed on the titania oxygen vacancy sides. Reduced titania modified with CuSO<sub>4</sub> (Figure 2c) showed a new band at 1448 cm<sup>−1</sup>, assigned to NO vibrations, which might be formed due to the oxidation of nitrogen species on the titania surface through the sulfate anions. The same band was observed in the reduced titania modified by Cu(NO<sub>3</sub>)<sub>2</sub> (Figure 2d). The asymmetric band at 1620 cm<sup>−1</sup> in the RT-Cu(NO<sub>3</sub>)<sub>2</sub> sample was probably a result of adsorption of Cu(NO<sub>3</sub>)<sub>2</sub> at the titania

surface defects. The adsorption of  $\text{Cu}(\text{OAc})_2$  on the reduced titania led to the decrease of the O–H band at  $1620\text{ cm}^{-1}$  and through this the surface became less hydrophilic. On the other hand, the adsorption of  $\text{CuSO}_4$  or  $\text{Cu}(\text{NO}_3)_2$  on the reduced titania caused the opposite effect; in these cases the hydrophilicity was increased. These FTIR studies showed the impact of titania surface defects on the attachment sites of various species from the copper salts.

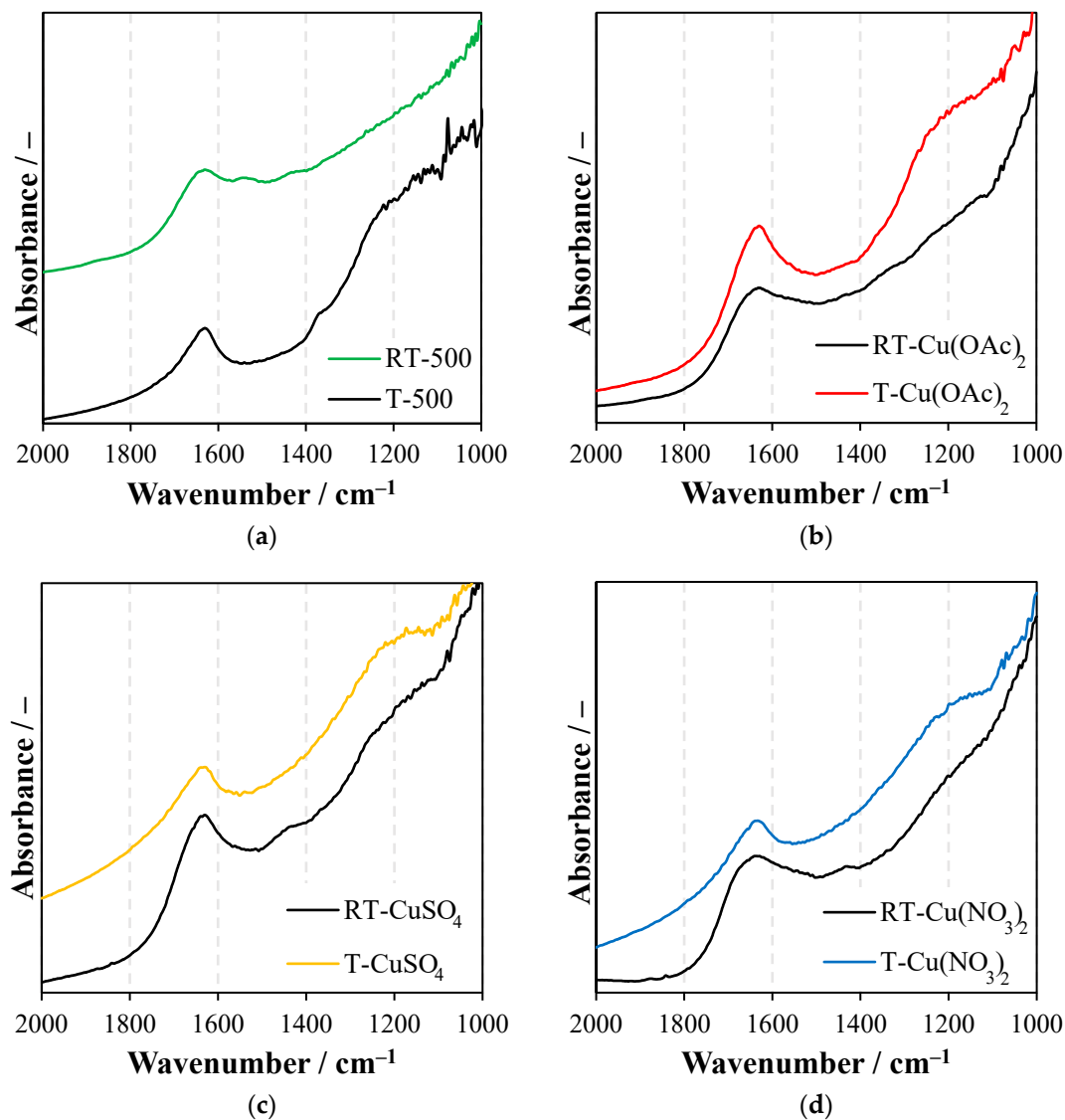


**Figure 2.** FTIR spectra of (a)  $\text{TiO}_2$  obtained in hydrothermal process with and without  $\text{NH}_4\text{OH}$  and heat-treated at  $500\text{ }^\circ\text{C}$ , RT-500 and T-500, respectively; (b) RT-500 and T-500 treated with  $\text{Cu}(\text{OAc})_2$ , (c) RT-500 and T-500 treated with  $\text{CuSO}_4$ , (d) RT-500 and T-500 treated with  $\text{Cu}(\text{NO}_3)_2$ .

#### 2.4. EPR Spectroscopy

EPR spectra of  $\text{TiO}_2$  samples obtained in two-step synthesis with an ammonia solution are illustrated in Figure 3. The first observed signal at 2.018 g-value refers to the surface-trapped holes ( $\text{Ti}^{4+}\text{O}^{2-}-\text{Ti}^{4+}\text{O}^{\bullet-}$ ) [24]. Signals at 2.002 g-value indicated the presence of electrons trapped in oxygen vacancies, whereas a signal at 1.929 was due to the presence of  $\text{Ti}^{3+}$  in rutile [25,26]. The signal at 1.983 g-value was assigned to trapped electrons in crystal lattice [24]. All of these samples revealed similar types of defects, but their intensity varied; in general, the intensities of all the spins decreased with an increased temperature of  $\text{TiO}_2$  heating. So,  $\text{TiO}_2$  heat-treated at  $500\text{ }^\circ\text{C}$  exhibited the most defected structure.

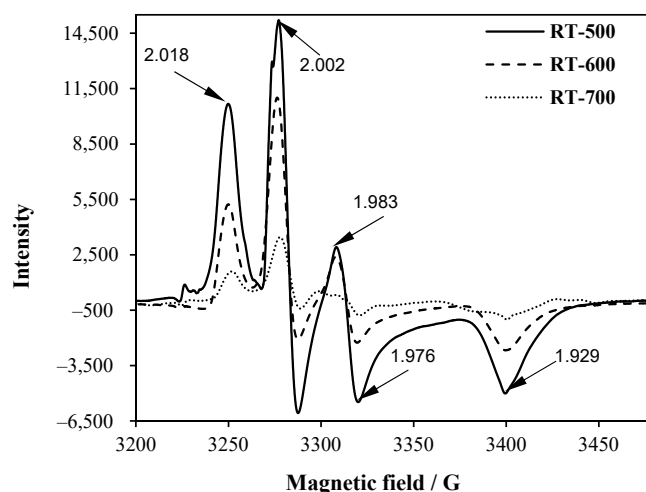


**Figure 3.** EPR spectra of reduced TiO<sub>2</sub> at 500, 600 and 700 °C. Tensor g values were added.

### 2.5. X-ray Photoelectron Spectroscopy

XPS measurements were performed to determine the ratio of Cu<sub>2</sub>O to CuO species in Cu-doped TiO<sub>2</sub> samples. Analyses of Ti2p and O1s binding energies were also examined and presented. The presence of inorganic residues in TiO<sub>2</sub> after Cu doping from copper salts was also considered in these analyses.

In Figure 4, XPS spectra of Cu2p<sub>3/2</sub> signals are presented, where Cu2p<sub>3/2</sub> was deconvoluted into two major peaks corresponding to CuO (red line) and Cu<sub>2</sub>O (blue line). The calculated peak area ratios of Cu<sub>2</sub>O to CuO in Cu-TiO<sub>2</sub> samples were listed in Table 3. In Figure 5, XPS spectra of Ti2p signals in RT-500 and Cu-doped TiO<sub>2</sub> samples were added; the values of binding energies were indicated in Table 3. In Figure 6, XPS spectra for S2p<sub>3</sub> signal in Cu-doped TiO<sub>2</sub> from CuSO<sub>4</sub> solution are illustrated.

The binding energy of Ti2p varied among the titania samples. The highest binding energy for Ti2p (459.14 eV) was noticed in titania modified with CuSO<sub>4</sub>.

According to the data reported in the literature [27], this effect can be related to the sulfur introduced to the crystal lattice of TiO<sub>2</sub>. However, in that studied in this research sample, it is considered that the presence of high amounts of SO<sub>4</sub><sup>2-</sup> bounded to the surface due to the applied method of Cu doping. Since the sulfur in this anion has a high oxidation state, the binding energy was shifted towards a higher value. A similar effect was also reported by the other researchers [28]. In the case of the RT-CuSO<sub>4</sub> sample, the binding energy for Ti2p was lower (458.57 eV) than in the case T-CuSO<sub>4</sub>, because a lower quantity of sulfate groups was attached to the titania surface. In Figure 5, XPS spectra of S2p signals for T-CuSO<sub>4</sub> and RT-CuSO<sub>4</sub> samples are shown. Two major peaks can be observed: (1) at the binding energy of 168 eV, which refers to S<sup>6+</sup> sulfur [29] and (2) at the binding energy of 163 eV, characteristic of S<sup>2-</sup> [6]. It can be clearly seen that modification of TiO<sub>2</sub> with an ammonia water effectively decreased the amount of sulfate species on its surface (mostly SO<sub>4</sub><sup>2-</sup>). All the titania samples, which were reduced with NH<sub>4</sub>OH and doped with Cu, showed a shifting of binding energies in Ti2p signals towards lower energies (Figure 5). This could be caused by the formation of Ti<sup>3+</sup> crystal lattice defects. A similar effect was reported by other researchers, who observed the presence of Ti<sup>3+</sup> defects as a weak shoulder in the Ti2p peak [30,31].

In Figure 7a–g, the XPS measurements of the O1s signal are shown. This signal was asymmetric and was deconvoluted into three peaks. To facilitate the comparison of these signals, the ratio of their peak areas was calculated. The highest intensity peak, with binding energy at around 530 eV, was ascribed to the crystal lattice oxygen Ti–O of TiO<sub>2</sub> (O<sub>lattice</sub>). The remaining signals were related to either Ti–OH species (O<sub>surface1</sub>) with binding energy at around 531 eV, hydroxyl groups adsorbed on the titania surface or acid residues derived from SO<sub>4</sub><sup>2-</sup>, NO<sub>3</sub><sup>-</sup> or –OAc groups [32,33]. The aforementioned last signal was located

with a binding energy which equaled around 532 eV ( $O_{\text{surface2}}$ ). First of all, the ratio of  $O_{\text{lattice}}/O_{\text{surface}}$  was calculated ( $O_{\text{surface}}$  means the sum of  $O_{\text{surface1}}$  and  $O_{\text{surface2}}$ ) and data were introduced in Table 3. It can be clearly seen that Cu-TiO<sub>2</sub> samples prepared by doping Cu to the reduced titania had a significantly higher ratio of lattice oxygen to the surface oxygen groups than the other ones. Next,  $O_{\text{surface1}}/O_{\text{surface2}}$  ratios were calculated. The middle oxygen signal ( $O_{\text{surface1}}$ ) of Ti–OH groups most likely comes from the adsorbed hydroxyl groups present at the oxygen vacancies' sides [32]. Therefore, Cu-TiO<sub>2</sub> samples prepared by doping Cu to the reduced titania had this more intensive signal in comparison to the other ones, because the oxygen vacancies were more numerous on the reduced titania surfaces. For example, TiO<sub>2</sub> reduced and treated with CuSO<sub>4</sub> (RT-CuSO<sub>4</sub>) indicated a much higher ratio of  $O_{\text{surface1}}/O_{\text{surface2}}$  (61/39) than that without preliminary reduction (T-CuSO<sub>4</sub>), with an oxygen surface ratio of 11/89.

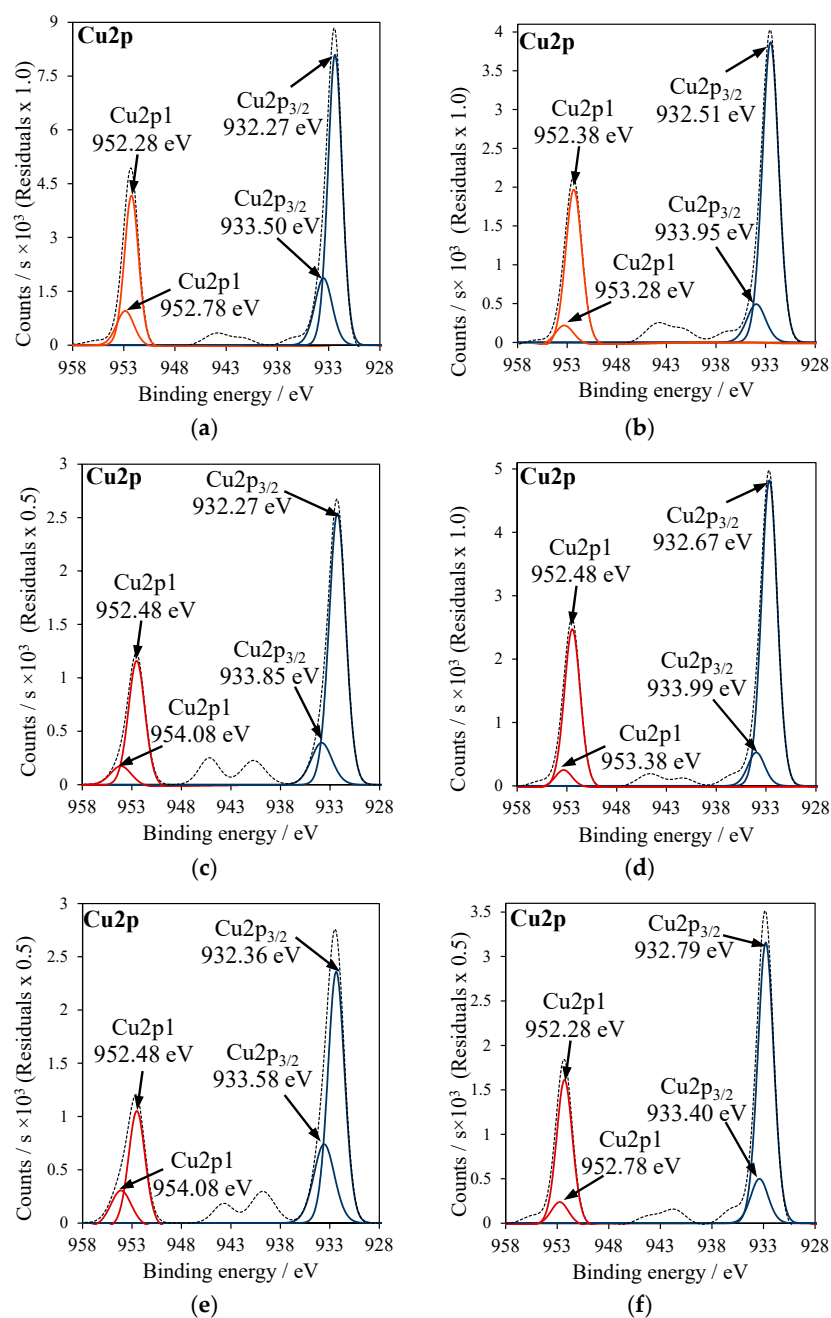


**Figure 4.** XPS spectra of Cu2p<sub>3/2</sub>: (a) RT-Cu(OAc)<sub>2</sub>, (b) RT-CuSO<sub>4</sub>, (c) RT-Cu(NO<sub>3</sub>)<sub>2</sub>, (d) T-Cu(OAc)<sub>2</sub>, (e) T-Cu(NO<sub>3</sub>)<sub>2</sub>, (f) T-CuSO<sub>4</sub>.

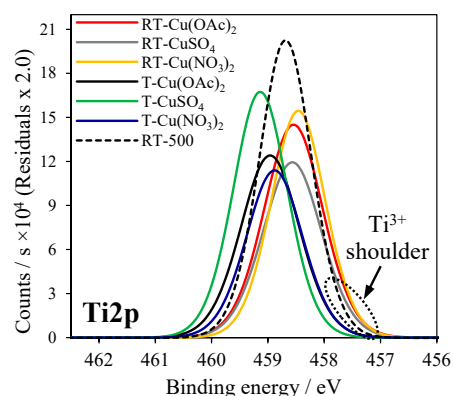


Figure 5. XPS spectra of Ti2p signals in RT-500 and Cu-TiO<sub>2</sub> samples.

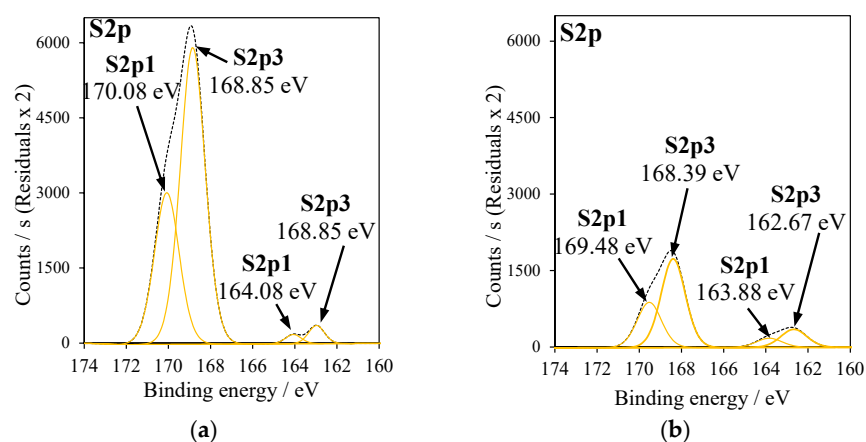


Figure 6. XPS spectra of S2p signals in (a) T-CuSO<sub>4</sub>, (b) RT-CuSO<sub>4</sub>.

Table 3. XPS analyses of RT-500 and Cu-TiO<sub>2</sub> samples.

Sample	Cu <sub>2</sub> O/CuO	O <sub>lattice</sub> /O <sub>surface</sub>	O <sub>surface1</sub> /O <sub>surface2</sub>	Ti2p BE/eV
RT-500	–	89.3/10.7	66.6/33.4	458.55
T-Cu(OAc) <sub>2</sub>	89.3/10.7	74.5/25.5	37.7/62.3	458.96
RT-Cu(OAc) <sub>2</sub>	77.9/22.1	83.6/16.4	68.2/31.8	458.55
T-CuSO <sub>4</sub>	86.2/13.8	71.2/28.8	10.8/89.2	459.14
RT-CuSO <sub>4</sub>	86.7/13.3	79.7/20.3	60.8/39.2	458.57
T-Cu(NO <sub>3</sub> ) <sub>2</sub>	71.9/28.1	70.1/29.9	34.4/65.6	458.88
RT-Cu(NO <sub>3</sub> ) <sub>2</sub>	84.0/16.0	78.4/21.6	40.8/59.2	458.46

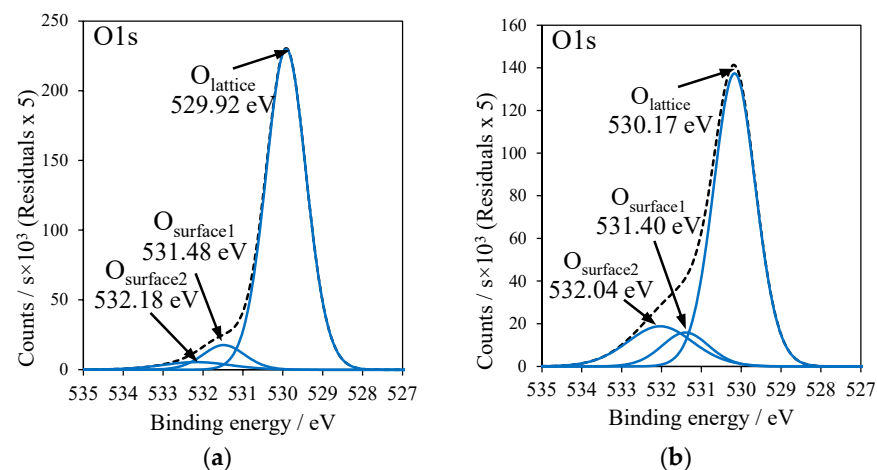
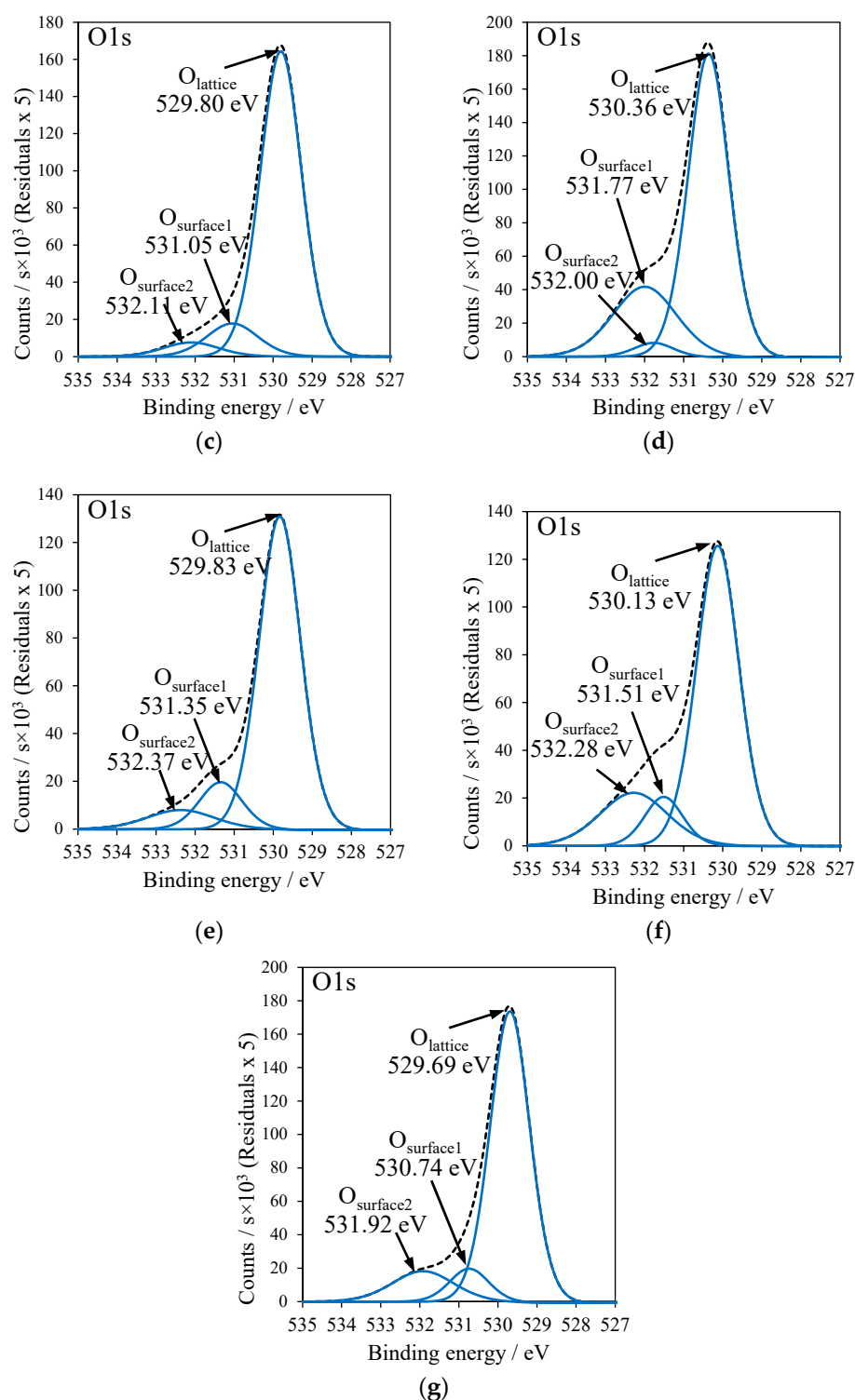


Figure 7. Cont.





**Figure 7.** XPS spectra of O1s: (a) RT-500, (b) T-Cu(OAc)<sub>2</sub>, (c) RT-Cu(OAc)<sub>2</sub>, (d) T-CuSO<sub>4</sub>, (e) RT-CuSO<sub>4</sub>, (f) T-Cu(NO<sub>3</sub>)<sub>2</sub>, (g) RT-Cu(NO<sub>3</sub>)<sub>2</sub>.

## 2.6. UV-Vis Spectroscopy

UV-Vis/DR spectroscopy measurements were performed in order to determine the optical properties of studied samples. In Figure 8a, UV-Vis/DR spectra of TiO<sub>2</sub> prepared upon NH<sub>4</sub>OH modification and following thermal heating at 500–700 °C are shown. Samples obtained at 500 °C showed enhanced absorption in the range of 390–450 nm, which could be related to the formation of some Ti<sup>3+</sup> centers and oxygen vacancies. A similar effect was

already observed in the other titania samples modified by  $\text{NH}_4\text{OH}$  [34]. A  $\text{TiO}_2$  sample heat-treated in  $700^\circ\text{C}$  (RT-700) indicated a slight shift of absorption shoulder towards the visible light range, which was caused by the formation of rutile. The modification of titania samples with Cu salts caused a significant change in the intensity of visible light absorption, as was illustrated in Figure 8b. The highest absorption in the visible range of 390–800 nm was RT-Cu(OAc) $_2$ , which was modified by Cu(OAc) $_2$ . This could be caused by the formation of carbon residues on the titania surface during carbonization of acetate groups at  $500^\circ\text{C}$ . In Figure 8c, the photos of the titania powders are illustrated. The RT-Cu(OAc) $_2$  sample indicated the most dark-brownish color. Reduced  $\text{TiO}_2$  treated with Cu(NO $_3$ ) $_2$  differs from the other titania samples in color, as it was greenish (Figure 8c).  $\text{TiO}_2$ -Cu samples obtained from the reduced titania showed maximum reflectance at around 500 nm, whereas the Cu- $\text{TiO}_2$  prepared from the titania pulp showed maximum reflectance at 600 nm. It can be concluded that  $\text{TiO}_2$ -Cu samples, which were prepared without pretreatment with  $\text{NH}_4\text{OH}$ , exhibited higher absorption in the visible range. This was caused by the higher quantity of oxygen surface groups adsorbed on the titania surface from the copper salts in these  $\text{TiO}_2$ -Cu samples by comparison with those obtained from the reduced  $\text{TiO}_2$ . These remarks are consistent with XPS analyses.

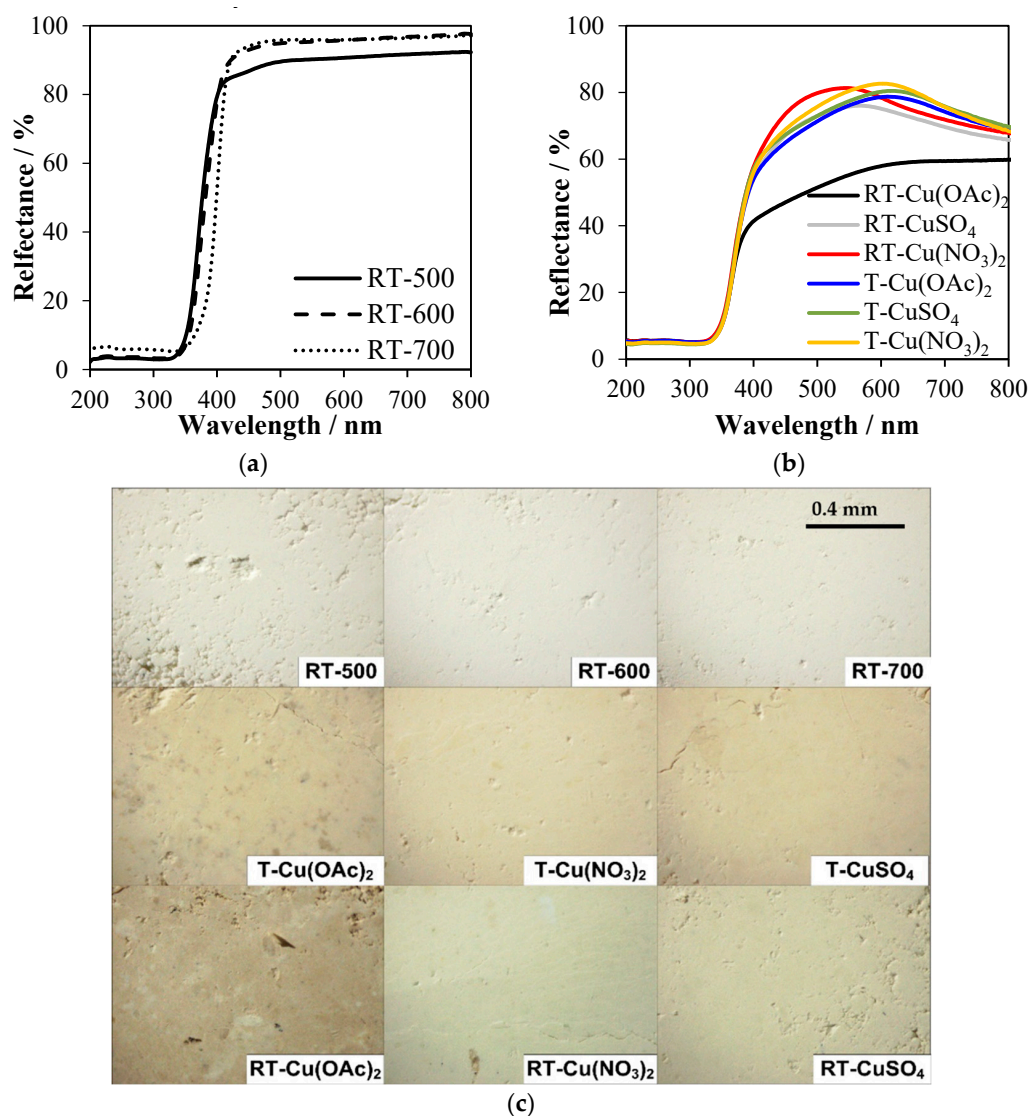


**Figure 8.** UV-Vis/DR spectra of (a)  $\text{TiO}_2$  modified with  $\text{NH}_4\text{OH}$ ; (b) Cu- $\text{TiO}_2$ ; (c) photos of titania powders taken using an optical microscope.

### 2.7. Zeta Potential and pH

Zeta potential was measured for titania powders suspended in an aqueous solution. Each time, the pH of aqueous suspension was measured because the acid or basic characteristics of titania surface and ionic strength could change the pH of the prepared solution. Zeta potential was measured in both saline (0.85% NaCl) and phosphate-buffered solutions to remodel the conditions used for the photocatalytic tests of bacteria inactivation. *E. coli* inactivation was carried out in a saline solution, but tests for *S. epidermidis* inactivation were performed in a phosphate buffer. Results from the measurements are presented in Table 4.

**Table 4.** Zeta potential and pH of Cu-TiO<sub>2</sub> samples.

Sample	Solution	pH	Zeta Potential/mV
RT-500		-	-12.43
RT-600		-	-9.15
RT-700		-	-10.78
T-Cu(OAc) <sub>2</sub>	NaCl	5.47	-7.23
RT-Cu(OAc) <sub>2</sub>		6.54	-7.37
T-CuSO <sub>4</sub>		4.43	-6.91
RT-CuSO <sub>4</sub>		6.18	-8.40
T-Cu(NO <sub>3</sub> ) <sub>2</sub>		4.48	-8.28
RT-Cu(NO <sub>3</sub> ) <sub>2</sub>		6.47	-11.50
RT-500			-
RT-600		-	-25.90
RT-700		-	-25.49
T-Cu(OAc) <sub>2</sub>	H <sub>3</sub> PO <sub>4</sub>	7.25	-24.60
RT-Cu(OAc) <sub>2</sub>		7.27	-24.90
T-CuSO <sub>4</sub>		7.24	-25.00
RT-CuSO <sub>4</sub>		7.24	-25.10
T-Cu(NO <sub>3</sub> ) <sub>2</sub>		7.23	-24.40
RT-Cu(NO <sub>3</sub> ) <sub>2</sub>		7.25	-26.00

Values of zeta potential measured in 0.85% NaCl solution varied among the samples, whereas in a phosphate buffer they were very similar. A TiO<sub>2</sub> sample modified with CuSO<sub>4</sub> without pretreatment with NH<sub>4</sub>OH showed the least negative zeta potential compared with the other samples in saline solution, and the lowest pH of solution which equaled 4.4. The acidic and polar character of titania oxygen surface groups increases adsorption of water molecules and can act to enhance hydroxyl radical formation. All the samples obtained with NH<sub>4</sub>OH modification had a more negative potential. Cu-doped TiO<sub>2</sub> samples using TiO<sub>2</sub> without NH<sub>4</sub>OH pretreatment showed a higher acidic surface, due to the presence of a higher quantity of surface oxygen groups, as was documented using XPS analyses. However, TiO<sub>2</sub> samples modified by Cu(OAc)<sub>2</sub> were more hydrophobic than the other ones due to the presence of carbonized groups on the surface. These samples indicated a lower change in pH solution, but in fact their zeta potential was around (-7 mV) which was less negative than for the TiO<sub>2</sub>-Cu samples obtained from a Cu(NO<sub>3</sub>)<sub>2</sub> precursor.

### 2.8. Antimicrobial Tests towards Escherichia Coli and Staphylococcus Epidermidis Inactivation in the Presence of Solar Light

In Figure 9, the results of the microbials test for pretreatment with NH<sub>4</sub>OH and heat-treatment at 500–700 °C under the solar lamp and in the darkness are presented. Almost all examined photocatalysts have very poor antibacterial properties without light activation. Under artificial solar irradiation, only T-500 samples promoted bacterial reduction with counts of around 2 log CFU mL<sup>-1</sup> after 30 min (Figure 9b,d). It is clear that the antibacterial activity of titania is directly correlated with its structural properties of photocatalysts. The T-500 sample is characterized by the smallest mean anatase crystallite sizes (17 nm). It is possible that such small particles penetrate inside the cells and cause an imbalance between

production and accumulation of oxygen reactive species (ROS), leading to harmful effects in important cellular structures such as proteins, lipids and nucleic acids.

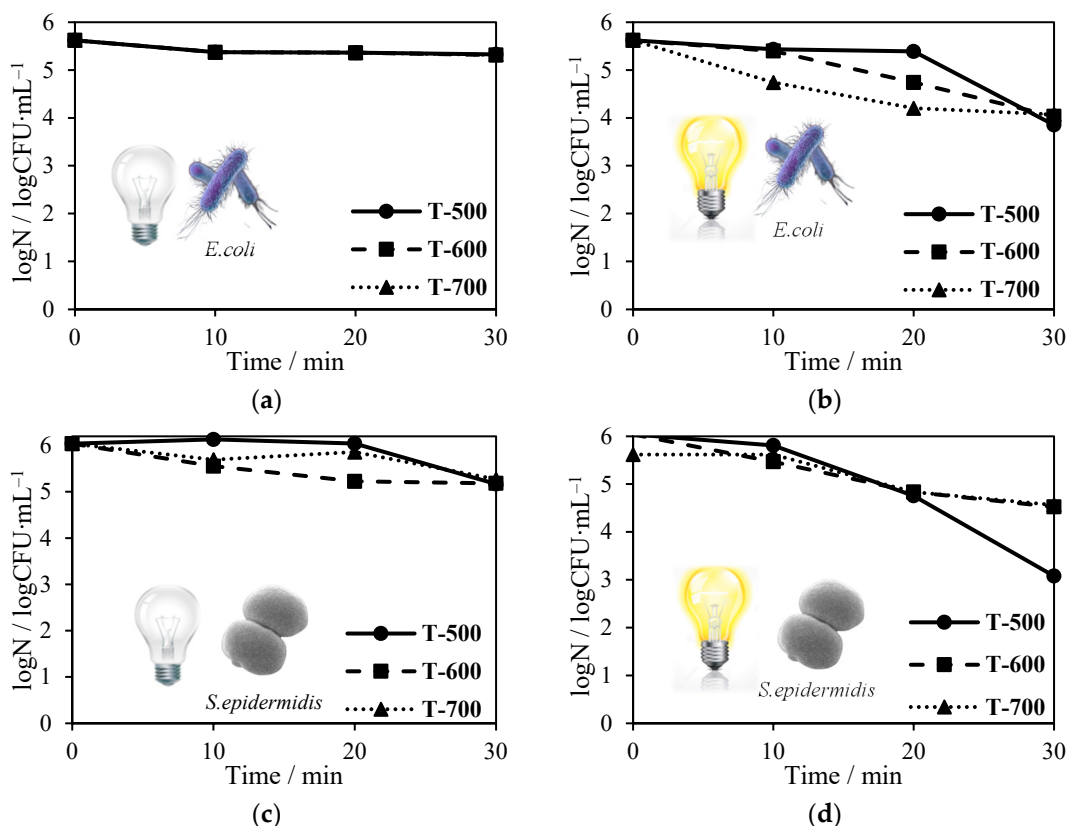


Figure 9. TiO<sub>2</sub> antimicrobial tests on *Escherichia coli* (a) in the absence of solar light and (b) in its presence; *Staphylococcus epidermidis* (c) in the absence of solar light (d) and in its presence.

According to Marugán et al. [35], photocatalytic-process bacteria are inactivated as a consequence of the cumulative effects of serial ROS attacks on the cell membrane–wall system and internal structures, that require a sufficient time. For that reason, we decided to conduct a test for reduced TiO<sub>2</sub> in a long period. The results are presented in Figure 10.

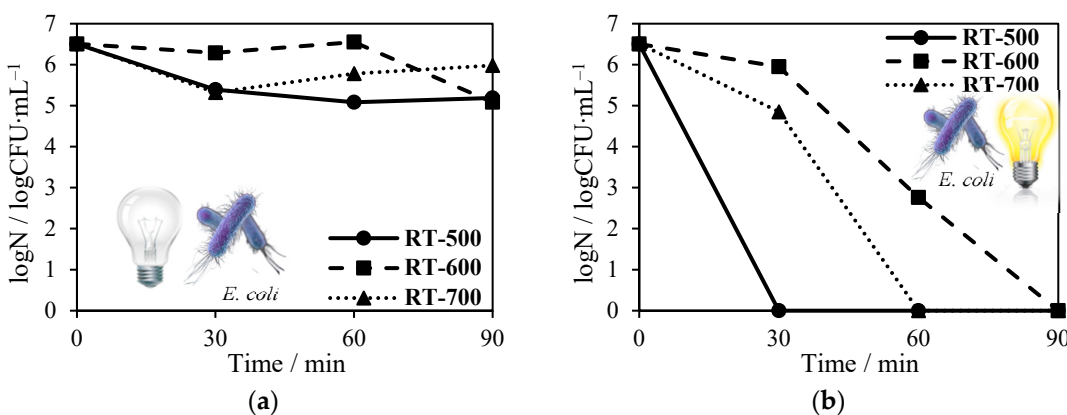
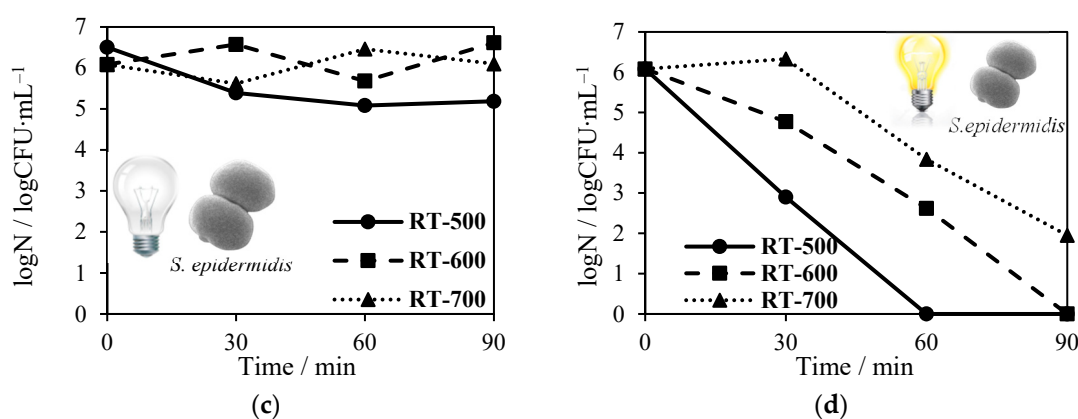


Figure 10. Cont.



**Figure 10.** Reduced TiO<sub>2</sub> antimicrobial tests on *Escherichia coli* (a) in the absence of solar light and (b) in its presence; *Staphylococcus epidermidis* (c) in the absence of solar light and (d) in its presence.

It can clearly be seen that regardless of tested photocatalyst or bacteria species, under dark conditions, even after 90 min, the decrease of bacterial number did not exceed 2 log CFU mL<sup>-1</sup>. The use of NH<sub>4</sub>OH and being heat-treated at 500, 600 and 700 °C TiO<sub>2</sub> against Gram-negative *E. coli* caused total inactivation after 30, 90 and 60 min, respectively. Complete removal of Gram-positive *S. epidermidis* (6 log reduction) was attained within 90 min of the total reaction only for RT-500 and RT-600 photocatalysts.

The impregnation of NH<sub>4</sub>OH and being heat-treated at 500–700 °C, or reduced TiO<sub>2</sub> samples with varied Cu salts, did not influence the antimicrobial properties in dark conditions (Figure 11a,c; Figure 13 a,c). The maximum 1 log reduction of the *E. coli* number was obtained for T-CuSO<sub>4</sub> (Figure 11a). However, under solar irradiation testing, photocatalysts have shown the opposite results. The most promising impregnation method seems to be the use of CuSO<sub>4</sub>. The shortest time (30 min) was required for total inactivation of *E. coli* and *S. epidermidis* during the process, in which T-CuSO<sub>4</sub> and RT-CuSO<sub>4</sub> were used. The slightly lower antimicrobial efficiency was obtained for T-Cu(NO<sub>3</sub>)<sub>2</sub> and RT-Cu(NO<sub>3</sub>)<sub>2</sub>, but only against Gram-positive *S. epidermidis* (Figure 12b,d). Unexpectedly, the worst results were from the wet impregnation with Cu(NO<sub>3</sub>)<sub>2</sub>·3H<sub>2</sub>O.

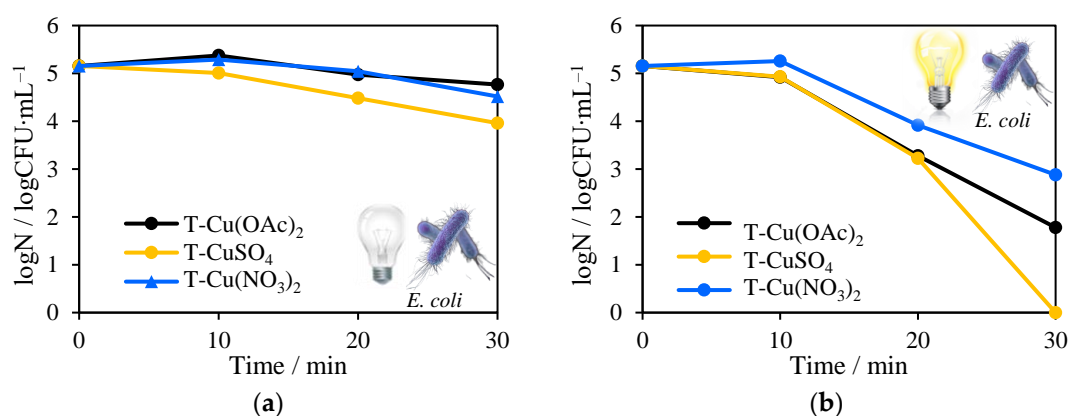


**Figure 11.** Cont.

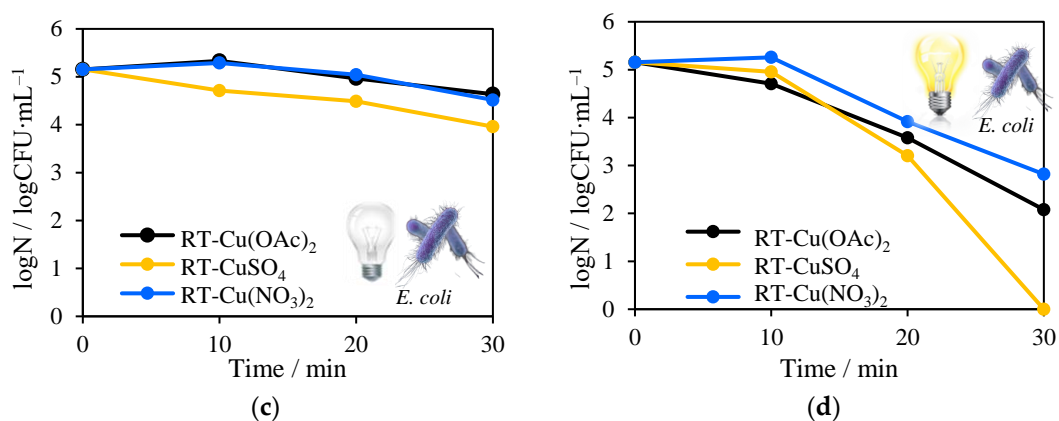


**Figure 11.** Antimicrobial tests with the addition of: Cu-TiO<sub>2</sub> on *Escherichia coli* in the absence of solar light (a) and in its presence (b); reduced Cu-TiO<sub>2</sub> in the absence of solar light (c) and in its presence (d).

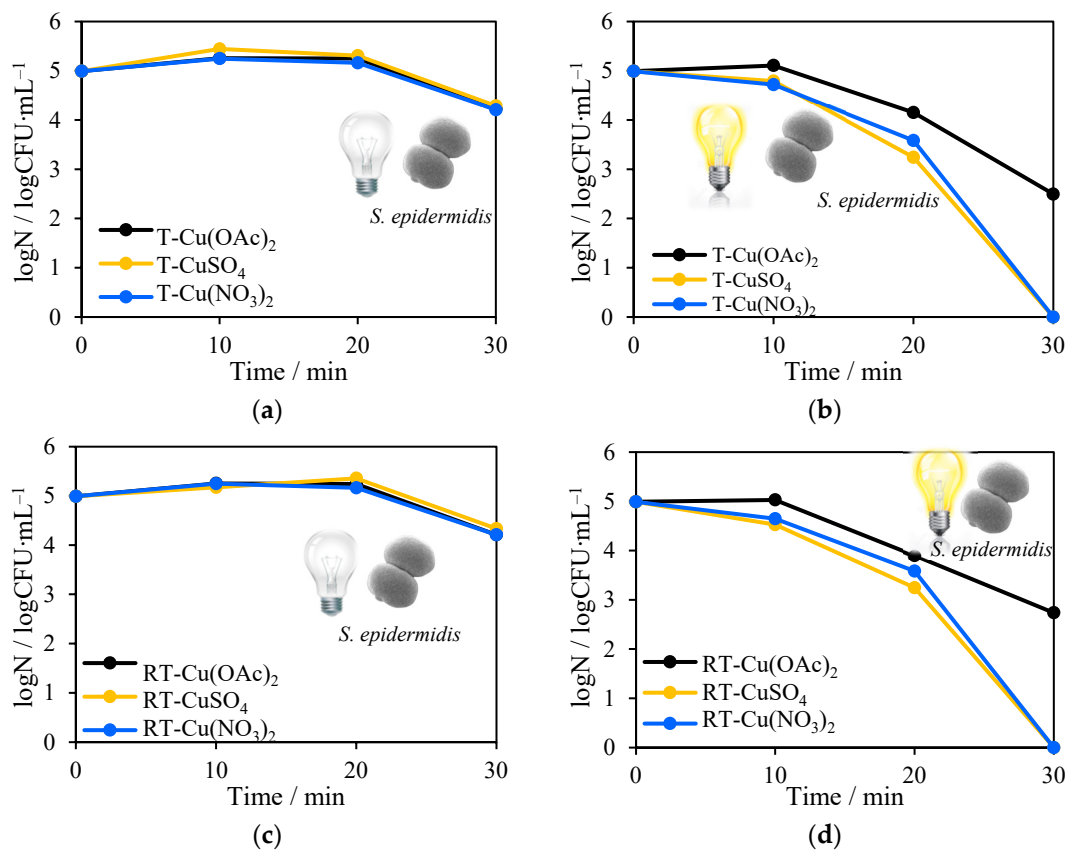


**Figure 12.** Antimicrobial tests with the addition of Cu-TiO<sub>2</sub> on *S. epidermidis* in the absence of solar light (a) and in its presence (b).

### 2.9. Reactive Radical Formation

In Figure 13, the detection of hydroxyl radicals formed in the presence of reduced TiO<sub>2</sub> are presented. In this method, concentration of 2-hydroxyterephthalic acid was monitored as a reaction product of hydroxyl radicals and terephthalic acid during UV irradiation of TiO<sub>2</sub>. It can clearly be seen that the highest efficiency of hydroxyl radicals was obtained in the case of the RT-500 sample and was much higher than in the reduced TiO<sub>2</sub> prepared at 600 and 700 °C. This experiment directly illustrates that the high quantity of hydroxyl radical formation on the RT-500 sample could impact on its higher antimicrobial

properties compared with the other reduced TiO<sub>2</sub> samples (Figure 10b,d). Moreover, the high amount of radicals formed could be strongly boosted by the presence of surface defects (see Figure 3).

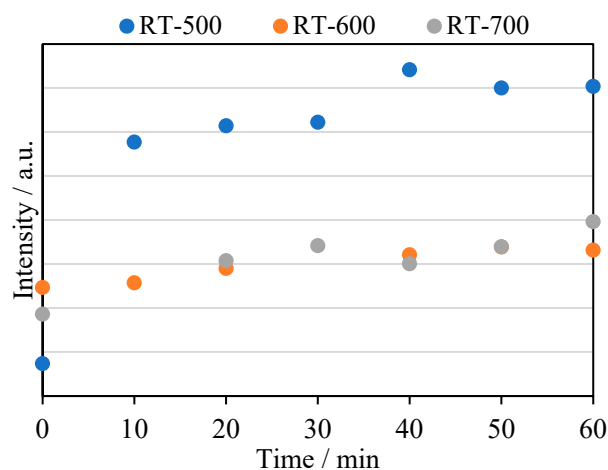


Figure 13. 2-HTA formation in the presence of reduced TiO<sub>2</sub> and ·OH radicals.

### 3. Discussion

The modification of a raw titania (originally containing sulfur in its composition) with an ammonia solution in autoclave at 150 °C introduced some of the ammonia species on the titania surface. The subsequent treatment of such a prepared sample at the temperatures of 500–700 °C caused the formation of some titania surface defects in the form of oxygen vacancies and Ti<sup>3+</sup> centers and electron traps at the titania lattice side. The most defected titania was obtained at 500 °C, just after the decomposition of surface-adsorbed ammonia species. At higher temperatures, rapid growing of anatase crystallites was observed and the mean size of anatase crystallites was changed from 21 to 57 nm during heat-treatment at 500 to 700 °C, respectively. The sulfate groups were also removed during the heating of titania pretreated with NH<sub>4</sub>OH. When we compare titania samples doped with Cu by using different copper salts with those titania reduced with ammonia and doped by using the same Cu precursors it is easy to observe the smaller quantity of sulfate species in TiO<sub>2</sub> pretreated with NH<sub>4</sub>OH. There is a high probability that ammonia species could form the ammonia sulfate compounds on the titania surface, which were decomposed during its heating at 500 °C. The addition of copper salt to the TiO<sub>2</sub> and its heating at 500 °C did not allow for the removal of sulfate species to such an extent as was noticed in TiO<sub>2</sub> treated with NH<sub>4</sub>OH. Moreover, a higher quantity of oxygen surface groups adsorbed on the titania surface was observed in the case of Cu-doped TiO<sub>2</sub> than the reduced one. However, reduced TiO<sub>2</sub> doped with Cu indicated a higher quantity of OH groups adsorbed on the titania vacancy sides. The amount of Cu doped to TiO<sub>2</sub> was comparable among all the samples with variation between 1.5 to 1.67 mass%. The ratio of Cu<sub>2</sub>O/CuO in the prepared titania samples was dependent on the copper salt used, and the highest being for CuSO<sub>4</sub> and Cu(CH<sub>3</sub>COO)<sub>2</sub>. In all the TiO<sub>2</sub>-doped Cu samples, Cu(I) was the dominant oxidation state, and the Cu<sub>2</sub>O/CuO ratio varied from 72/28 to 89/11. Inactivation of two bacteria species, Gram-negative *E. coli* and Gram-positive *S. epidermidis*, was assayed with reduced TiO<sub>2</sub> (RT), TiO<sub>2</sub>-doped Cu (T-Cu) and TiO<sub>2</sub> reduced and doped with Cu (RT-Cu). Both TiO<sub>2</sub> reduction and Cu doping on TiO<sub>2</sub> were effective for improving the antibacterial properties of TiO<sub>2</sub>. However, a synergistic effect for TiO<sub>2</sub> with double modification (NH<sub>4</sub>OH and Cu doping) was not observed. The most likely inactivation of bacteria by reduced TiO<sub>2</sub> occurs through a different mechanism than in the case of TiO<sub>2</sub> doped with Cu species. Copper can be very toxic for microorganisms mainly due to ‘contact killing’ mechanisms [13]. In the case of reduced TiO<sub>2</sub> obtained by modification with NH<sub>4</sub>OH, the main route of bacteria inactivation can go through the formation of oxygen radicals on titania surfaces upon

its excitation with UV light. Formed reactive radicals can oxidize outer membranes (cell wall and cell membrane) and then damage internal cellular structures. The presence of  $Ti^{3+}$  centers in  $TiO_2$  can increase its hydrophilicity and contribute to hydroxyl radicals' formation, which have a very high potential for oxidation. Metallic copper can be released from the photocatalyst and can penetrate through the partially damaged membrane cells of bacteria up to cytoplasm and then cause oxidative stress and DNA degradation. These studies showed that Cu-doped  $TiO_2$  obtained from the  $CuSO_4$  precursor had the higher antibacterial potential against both species, *E. coli* and *S. epidermidis*. It is considered that some sulfate species remaining on the  $TiO_2$  surface could have a positive effect on increasing bacterial adhesion. According to Oh et al., many factors are responsible for this process; the most important ones include changes in the van der Waals force and electrostatic double-layer interactions or acid-base interactions, and increasing hydrophobicity [36].

Both the impregnation method, as well as a type of isotonic solution utilized in the experiments (NaCl or PBS), can cause changes in the nature of the obtained photocatalysts' surface. It was shown that in 0.85% NaCl, the photocatalysts' zeta potentials were more varied and depended on the electronic charge distribution on the photocatalyst surface, while in PBS buffer the potential differences between samples were negligible (Table 4). It is a well-known fact that the zeta potential of a surface plays an important role on the adsorption of aqueous contaminants, including bacteria, on it [37]. A higher surface charge (less negative potential) facilitates the adhesion of the bacteria to the photocatalyst, which enhances antimicrobial potential [38,39]. The electrostatic behavior of the charge-regulated surfaces of Gram-negative and Gram-positive bacteria depends on characteristic properties of cell-wall functional groups. The charge regulations allow bacteria to respond to changes in solution pH and electrolyte composition. According to Hu et al. [40], a higher *E. coli* inactivation rate was obtained at  $pH > 5.1$ . This is due to the electrostatic repulsive forces between the bacteria and the light-activated photocatalyst, which have increasing pH due to the more negative zeta potential. A similar result was obtained in our study. At a pH range of 3 to 5, more positively charged photocatalyst particles can faster diffuse to the bacteria surface and cause its inactivation. The highest activity for *E. coli* inactivation was revealed for the T- $CuSO_4$  sample, with a zeta potential equal to  $-6.91$  mV, then for T- $Cu(OAc)_2$ , with a zeta potential of  $-7.25$  mV, and the worst was T- $Cu(NO_3)_2$ , with a zeta potential of  $-8.28$  mV. In the case of the *S. epidermidis* species, almost all of the titania samples showed complete inactivation of this bacteria within 30 min of solar light irradiation with the exception of the T- $Cu(OAc)_2$ , which contained the lowest quantity of sulfates among all the samples prepared from the titania pulp without undergoing the pretreatment process with  $NH_4OH$ . In the case of  $TiO_2$ -Cu-doped photocatalysts prepared from the reduced titania, bacteria inactivation was probably highly supported by the radical mechanism. It is well known that the Gram-negative *E. coli* bacteria is slightly more resistant to photocatalytic process, owing to their unique cell wall structure. This is due to the lower peptidoglycan content and lipopolysaccharide (LPS) outer membrane. It was shown that pH plays an imperative role in increasing photocatalytic efficiency under artificial solar light.

## 4. Materials and Methods

### 4.1. Materials

Two-step synthesis was conducted in order to obtain reduced  $TiO_2$  photocatalysts. In the first step, water suspension of raw titania obtained from the chemical factory Grupa Azoty S.A. Police (Police, Poland) was heated at  $150$  °C under naturally increased pressure of approximately 7.4 bar for 1 h. In this step, the ammonia water solution was added to autoclave with pH regulation up to 10. In the second step, obtained pre-crystallized titania was transferred to the pipe furnace and heat-treated at either 500, 600 or 700 °C under the flow of argon ( $20$  mL  $min^{-1}$ ) for 2 h. A heating rate of  $10$  °C/min was applied. The flowchart of  $TiO_2$  preparation was presented in Figure 14.



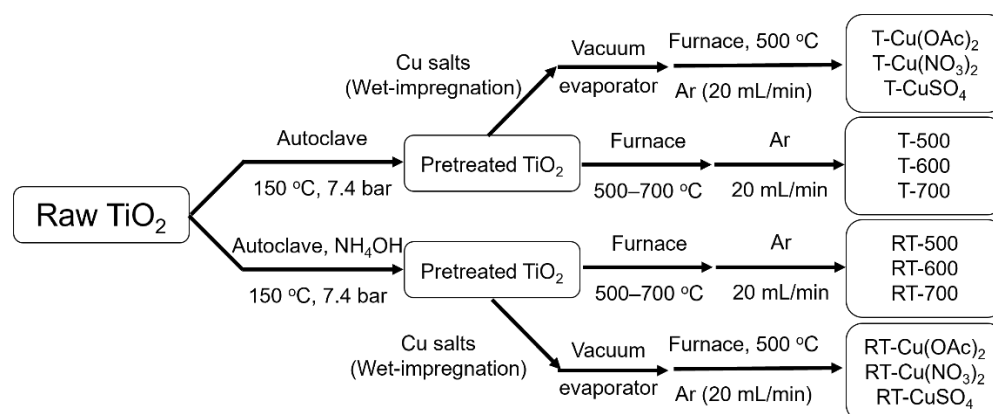


**Figure 14.** Preparation of reduced TiO<sub>2</sub> (middle section) and Cu-TiO<sub>2</sub> photocatalysts (outer sections).

Three-step synthesis of Cu-TiO<sub>2</sub> photocatalysts was conducted, where the first step was similar to that discussed previously: pre-crystallization of raw titania in a water suspension with or without the addition of ammonia water at 150 °C; 7.4 bar for 1 h. Obtained samples were then wet-impregnated with Cu(CH<sub>3</sub>COO)<sub>2</sub>·H<sub>2</sub>O (later marked as Cu(OAc)<sub>2</sub>), CuSO<sub>4</sub>·5H<sub>2</sub>O or Cu(NO<sub>3</sub>)<sub>2</sub>·3H<sub>2</sub>O water solutions in a rotary vacuum evaporator at the temperature of 60 °C and pressure of 200 mbar, until the complete evaporation of the solvent occurred. The addition of copper salt was calculated, so the final product theoretically had 1.0 wt% of Cu content. For example, to obtain a T-CuSO<sub>4</sub> sample, 4 g of pre-treated TiO<sub>2</sub> was mixed with 156 mg of CuSO<sub>4</sub>·5H<sub>2</sub>O as the sulfate group and 5 water molecules had to be taken into account. The last step of synthesis covered heat-treatment of TiO<sub>2</sub> previously impregnated with Cu salt in a pipe furnace at 500 °C under the flow of argon (20 mL min<sup>-1</sup>) for 2 h. A heating rate of 10 °C/min was applied. The flowchart of preparation of Cu-TiO<sub>2</sub> photocatalysts was presented in Figure 14.

#### 4.2. Methods

Electron paramagnetic resonance (EPR) was conducted in order to define both the presence and amount of titania surface defects. EPR spectra were measured in quartz tubes under inert gas atmosphere at the temperature of −196 °C, using a JEOL JES-X310 Electron Spin Resonance Spectrometer (Tokyo, Japan).

FT-IR measurements were performed using reflection techniques in air atmosphere, using Jasco FTIR 4200 (Tokyo, Japan). Spectra were measured with a scanning speed of 1 nm/sec, resolution of 4 cm<sup>-1</sup>. The background was measured at first and then each time it was subtracted prior to sample measurement.

X-ray photoelectron spectroscopy (XPS) measurements were performed using Thermo-Scientific K-Alpha XPS System (Waltham, MA, USA) 1486.6 eV Al K<sub>α</sub> X-ray source with a pass energy of 50 eV. A scan step of 0.1 eV was applied, irradiating 400 μm of the sample. Binding energy (B.E.) values were adjusted to the C1s transition (284.6 eV).

UV-Vis/DRS spectroscopy was used to investigate the optical properties of prepared TiO<sub>2</sub> samples. These measurements were carried out in a V-650 Jasco Spectrometer (Tokyo, Japan). The spectra were recorded in the UV-Vis range of 200–800 nm (scan rate of 1 nm/s). A pure block of BaSO<sub>4</sub> was used as a reference.

TEM images were taken using JEOL, JEM-2010 200 keV, with a GATAN ORIUS SC600 camera and GATAN Digital Micrograph 1.80.70 for GMS 1.8.0. Images of Cu-TiO<sub>2</sub> samples have been included as supplementary materials (Figures S1–S6).

X-ray diffraction measurements (XRD) were performed with an Empyrean Diffractometer PANalytical (Almelo, Netherlands), using a copper lamp (λ = 0.154439 nm). Measurements were carried out with the setting of Cu lamp parameters of 35 kV and

30 mA. The mean crystallite size of both anatase and rutile phases were calculated from the Scherrer Equation:

$$D = \frac{K \cdot \lambda}{(\beta - b) \cdot \cos \theta} \quad (1)$$

where  $K$  is the shape factor ( $K = 0.93$ ),  $\lambda$  is the wavelength of Cu lamp (nm),  $\beta$  is the width of the peak at half the maximum intensity after subtraction of background (rad),  $b$  is the apparatus dilatation (rad) and  $\theta$  is the diffraction angle ( $^{\circ}$ ).

The percentage amount of both copper and sulfur contents in  $\text{TiO}_2$  were measured using an energy dispersive X-ray fluorescence (EDXRF) spectrometer Epsilon3, Malvern PANalytical, (Almelo, Netherlands), using an internal pattern.

Both zeta potential and pH measurements were performed using Malvern PANalytical Zetasizer Nano-ZS (Almelo, Netherlands). For measurement, two types of titania suspensions were prepared. The first one was in NaCl solution with the same concentration as was used for the inactivation test of *E. coli* and the second one was in  $\text{H}_3\text{PO}_4$  buffer, which was used during the inactivation test of *S. epidermidis*. Each time, 20 mg of the given photocatalyst was dispersed into 100 mL of solution, using an ultrasonic bath (15 min). The pH of suspension was measured using a pH-responsive electrode, previously calibrated by three different buffers: acidic, neutral and basic. Such prepared suspensions were transferred to the specially designed, electro-conducting measurement cells, where zeta potential was measured.

The antibacterial properties of the tested photocatalysts were determined by measuring the inactivation rate of Gram-negative *Escherichia coli* K12 ATCC 25992 and Gram-positive *Staphylococcus epidermidis* ATCC 49461 bacteria in the reaction suspension. The frozen bacterial cultures in 15% glycerol and appropriate freezing media were placed in a water bath at  $37^{\circ}\text{C}$  for 5 min. Bacteria was suspended in a suitable strain liquid medium (Nutrient Broth for *E. coli* or BHI Broth for *S. epidermidis*, BioMaxima Sp. z o.o, Lublin, Poland) and incubated for 24 h at  $37^{\circ}\text{C}$ . The solution was decanted using ultracentrifuge (5000 RPM) and the remaining bacterial pellet was diluted with a sterile isotonic saline solution containing 0.85% NaCl (Chempur, Piekary Slaskie, Poland) for *Escherichia coli* bacteria or phosphate-buffered saline PBS (Chempur, Piekary Slaskie, Poland) for *Staphylococcus epidermidis*. The McFarland densitometer DEN-1 (Biosan, Riga, Latvia) was used to determine the optical density OD ( $\lambda = 600$  nm) of bacterial suspensions. Dilution was adjusted to 0.5 McFarland turbidity standard to achieve bacterial suspension of  $1.5 \times 10^8$  CFU  $\text{cm}^{-3}$ . A tested photocatalyst was added to a glass bottle containing 250  $\text{cm}^3$  of the started suspensions in saline or PBS buffer. The concentration of photocatalysts was  $0.1 \text{ g dm}^{-3}$ . Then, 100  $\text{cm}^3$  of each of the resulting suspensions of bacteria and photocatalyst were measured in glass reactors equipped with a magnetic stirrer. The entire set-up was placed on a magnetic stirrer under a UV-VIS-emitting lamp (ULTRA-VITALUX 230V E27/ES, OSRAM 300W, Munich, Germany). The stirring speed was 200 RPM. At the same time, an identically prepared experimental set was placed in an incubator without a light source (in the dark). In both cases, the temperature was maintained at  $37^{\circ}\text{C}$ . Control experiments were carried out in the same way, without the addition of a photocatalyst, for bacterial suspensions in saline or PBS. The experiments were conducted for 30 min. In order to determine the number of viable bacteria in the reaction suspension, 0.5  $\text{cm}^3$  of the reaction suspension was taken after 0, 10, 20 and 30 min. The collected sample was diluted according to the decimal dilution scheme. A saline solution (0.85% NaCl) for *E. coli* or PBS buffer for *S. epidermidis* was used to prepare the dilutions. Then, 0.25  $\text{cm}^3$  of the suspensions at the appropriate concentrations were placed in Petri dishes with sterile medium Plate Count Agar (PCA, BioMaxima Sp. z o.o, Lublin, Poland) for *E. coli* or Brain Heart Infusion agar (BHI, BTL Sp. z o.o, Lodz, Poland) for *S. epidermidis*. After the application of the suspension, the plates were incubated at  $37^{\circ}\text{C}$  for 24 h. After this time, the visible bacterial colonies were counted as  $\log \text{CFU mL}^{-1}$ . The results were presented as a percentage of surviving bacteria remaining after the process.

The detection of  $\cdot\text{OH}$  radical formation on the  $\text{TiO}_2$  surface was performed using the fluorescence technique. In this method, transformation of terephthalic acid (TA) to 2-hydroxyterephthalic acid (2-HTA) was carried out in the presence of  $\text{TiO}_2$  and UV irradiation. The concentration of TA used was  $5 \times 10^{-4} \text{ mol}\cdot\text{dm}^{-3}$ , sample weight was 20 mg and the solution volume was  $100 \text{ cm}^3$ . Additionally, to simulate the bacteria environment, NaCl (0.85%) was added to the reaction solution. As a source of UV light, an LED UV lamp composed of three LED diodes (10 W) was used. The concentration of 2-HTA was analyzed using a fluorescence spectrophotometer (Hitachi, F-2500, Japan, Kyoto).

## 5. Conclusions

The modification of  $\text{TiO}_2$  with  $\text{NH}_4\text{OH}$  and the following heat-treatment at 500–700 °C conducts the formation of some titania surface defects such as oxygen vacancies and  $\text{Ti}^{3+}$  centers, with higher quantities at high temperatures. The presence of oxygen surface defects in  $\text{TiO}_2$  increases its antimicrobial properties. The presence of titania surface defects increases its hydrophilicity and adsorption of hydroxyl groups, which is beneficial for OH radical formation. However, high adsorption of hydroxyl ions can change the potential charge of titania surface into negative ones. The negative zeta potential of  $\text{TiO}_2$  hinders its diffusion to *E. coli* species and can weaken its killing potential. The wet impregnation of  $\text{TiO}_2$  with copper salts and following heat-treatment at 500 °C under argon atmosphere led to the significant reduction of Cu(II) to a Cu(I) oxidation state. However, the type of copper precursor used influenced its antimicrobial properties more than the amount of Cu(I) on the  $\text{TiO}_2$  surface. The  $\text{CuSO}_4$  precursor appeared to be the best copper compound in the enhancement of antimicrobial properties of  $\text{TiO}_2$  in two bacteria species, *E. coli* and *S. epidermidis*. Additionally, obtained in this way,  $\text{TiO}_2$  photocatalyst contained the sulfur species, which could act as the toxic agent for microorganisms, as well. Moreover, such a prepared T- $\text{CuSO}_4$  sample has an acidic surface and is hydrophilic with a high potential for the generation of reactive radicals. The addition of T- $\text{CuSO}_4$  sample to a saline solution changes the pH into more acidic. By decreasing the pH of the solution, the zeta surface charge of  $\text{TiO}_2$  changes to become more positive. Therefore, it is concluded that the acidic surface, high hydrophilicity and the presence of Cu(I) in  $\text{TiO}_2$  increase its antimicrobial properties.

**Supplementary Materials:** The following supporting information can be downloaded at: <https://www.mdpi.com/article/10.3390/molecules27249032/s1>, Figure S1. TEM images of RT-500; Figure S2. TEM images of RT-Cu(OAc)<sub>2</sub>; Figure S3. TEM images of RT-CuSO<sub>4</sub>; Figure S4. TEM image of RT-Cu(NO<sub>3</sub>)<sub>2</sub>; Figure S5. TEM images of T-Cu(OAc)<sub>2</sub>; Figure S6. TEM images of T-Cu(NO<sub>3</sub>)<sub>2</sub>; Figure S7. TEM images of T-CuSO<sub>4</sub>.

**Author Contributions:** P.R.: investigation, data curation, writing—original draft preparation, visualization, funding acquisition, project administration; M.C.R.-M.: supervising, methodology, data curation; M.Á.L.-R.: data curation; O.P.: investigation, formal analysis; A.M.-S.: writing—review and editing, formal analysis; B.T.: conceptualization, methodology, validation, supervision, writing—original draft preparation, writing—review and editing. All authors have read and agreed to the published version of the manuscript.

**Funding:** This research was funded by the West Pomeranian University of Technology in Szczecin Rector Grant for PhD students of Doctoral School; grant number ZUT/29/2022.

**Institutional Review Board Statement:** Not applicable.

**Informed Consent Statement:** Not applicable.

**Data Availability Statement:** Not applicable.

**Acknowledgments:** The authors would like to thank both the research group of the University of Alicante and the technical staff for performing the XPS and TEM analyses and supporting their interpretation; Paula Felczak for help in samples preparation; Piotr Miądlicki for performing XRD analysis; and Joanna Sreńscek-Nazzal for performing XRF analysis.

**Conflicts of Interest:** The authors declare no conflict of interest.

**Sample Availability:** Samples of the compounds are not available from the authors.

## References

1. Leung, Y.H.; Xu, X.; Ma, A.P.Y.; Liu, F.; Ng, A.M.C.; Shen, Z.; Gethings, L.A.; Guo, M.Y.; Djurišić, A.B.; Lee, P.K.H.; et al. Toxicity of ZnO and TiO<sub>2</sub> to Escherichia Coli Cells. *Sci. Rep.* **2016**, *6*, 35243. [[CrossRef](#)]
2. Chen, S.; Guo, Y.; Chen, S.; Ge, Z.; Yang, H.; Tang, J. Fabrication of Cu/TiO<sub>2</sub> Nanocomposite: Toward an Enhanced Antibacterial Performance in the Absence of Light. *Mater. Lett.* **2012**, *83*, 154–157. [[CrossRef](#)]
3. Rahmawati, F.; Kusumaningsih, T.; Hapsari, A.; Hastuti, A. Ag and Cu Loaded on TiO<sub>2</sub>/Graphite as a Catalyst for Escherichia Coli-Contaminated Water Disinfection. *Chem. Pap.* **2010**, *64*, 557–565. [[CrossRef](#)]
4. Rizzo, L.; Sannino, D.; Vaiano, V.; Sacco, O.; Scarpa, A.; Pietrogiamomi, D. Effect of Solar Simulated N-Doped TiO<sub>2</sub> Photocatalysis on the Inactivation and Antibiotic Resistance of an *E. Coli* Strain in Biologically Treated Urban Wastewater. *Appl. Catal. B Environ.* **2014**, *144*, 369–378. [[CrossRef](#)]
5. Lee, H.U.; Lee, S.C.; Choi, S.; Son, B.; Lee, S.M.; Kim, H.J.; Lee, J. Efficient Visible-Light Induced Photocatalysis on Nanoporous Nitrogen-Doped Titanium Dioxide Catalysts. *Chem. Eng. J.* **2013**, *228*, 756–764. [[CrossRef](#)]
6. Lei, X.F.; Xue, X.X.; Yang, H.; Chen, C.; Li, X.; Niu, M.C.; Gao, X.Y.; Yang, Y.T. Effect of Calcination Temperature on the Structure and Visible-Light Photocatalytic Activities of (N, S and C) Co-Doped TiO<sub>2</sub> Nano-Materials. *Appl. Surf. Sci.* **2015**, *332*, 172–180. [[CrossRef](#)]
7. Janczarek, M.; Kowalska, E. Defective Dopant-Free TiO<sub>2</sub> as an Efficient Visible Light-Active Photocatalyst. *Catalysts* **2021**, *11*, 978. [[CrossRef](#)]
8. Rychtowski, P.; Tryba, B.; Skrzypaska, A.; Felczak, P.; Sreńscek-Nazzal, J.; Wróbel, R.J.; Nishiguchi, H.; Toyoda, M. Role of the Hydroxyl Groups Coordinated ToTiO<sub>2</sub> Surface on the Photocatalytic Decomposition of Ethylene at Different Ambient Conditions. *Catalysts* **2022**, *12*, 386. [[CrossRef](#)]
9. Rychtowski, P.; Tryba, B.; Fuks, H.; Lillo-Ródenas, M.Á.; Román-Martínez, M.C. Impact of TiO<sub>2</sub> Surface Defects on the Mechanism of Acetaldehyde Decomposition under Irradiation of a Fluorescent Lamp. *Catalysts* **2021**, *11*, 1281. [[CrossRef](#)]
10. Rychtowski, P.; Orlikowski, J.; Żotnierkiewicz, G.; Tryba, B. Mechanism of Hydroxyl Radicals Formation on the Reduced Rutile. *Mater. Res. Bull.* **2022**, *147*, 111643. [[CrossRef](#)]
11. Zhang, J.; Liu, S.; Wang, X.; Yao, J.; Zhai, M.; Liu, B.; Liang, C.; Shi, H. Highly Efficient Ti<sup>3+</sup> Self-Doped TiO<sub>2</sub> Co-Modified with Carbon Dots and Palladium Nanocomposites for Disinfection of Bacterial and Fungi. *J. Hazard. Mater.* **2021**, *413*, 125318. [[CrossRef](#)] [[PubMed](#)]
12. Zhang, J.; Yuan, M.; Liu, X.; Wang, X.; Liu, S.; Han, B.; Liu, B.; Shi, H. Copper Modified Ti<sup>3+</sup> Self-Doped TiO<sub>2</sub> Photocatalyst for Highly Efficient Photodisinfection of Five Agricultural Pathogenic Fungus. *Chem. Eng. J.* **2020**, *387*, 124171. [[CrossRef](#)]
13. Vincent, M.; Duval, R.E.; Hartemann, P.; Engels-Deutsch, M. Contact Killing and Antimicrobial Properties of Copper. *J. Appl. Microbiol.* **2018**, *124*, 1032–1046. [[CrossRef](#)]
14. Lopez, T.; Cuevas, J.L.; Ilharco, L.; Ramírez, P.; Rodríguez-Reinoso, F.; Rodríguez-Castellón, E. XPS Characterization and *E. Coli* DNA Degradation Using Functionalized Cu/TiO<sub>2</sub> Nanobiocatalysts. *Mol. Catal.* **2018**, *449*, 62–71. [[CrossRef](#)]
15. Rtimi, S.; Baghriche, O.; Pulgarin, C.; Lavanchy, J.-C.; Kiwi, J. Growth of TiO<sub>2</sub>/Cu Films by HiPIMS for Accelerated Bacterial Loss of Viability. *Surf. Coat. Technol.* **2013**, *232*, 804–813. [[CrossRef](#)]
16. Wang, K.; Bielan, Z.; Endo-Kimura, M.; Janczarek, M.; Zhang, D.; Kowalski, D.; Zielińska-Jurek, A.; Markowska-Szczupak, A.; Ohtani, B.; Kowalska, E. On the Mechanism of Photocatalytic Reactions on Cu<sub>x</sub>O@TiO<sub>2</sub> Core-Shell Photocatalysts. *J. Mater. Chem. A* **2021**, *9*, 10135–10145. [[CrossRef](#)]
17. Yang, X.; Wang, S.; Sun, H.; Wang, X.; Lian, J. Preparation and Photocatalytic Performance of Cu-Doped TiO<sub>2</sub> Nanoparticles. *Trans. Nonferrous Met. Soc. China* **2015**, *25*, 504–509. [[CrossRef](#)]
18. Miao, Y.; Xu, X.; Liu, K.; Wang, N. Preparation of Novel Cu/TiO<sub>2</sub> Mischcrystal Composites and Antibacterial Activities for Escherichia Coli under Visible Light. *Ceram. Int.* **2017**, *43*, 9658–9663. [[CrossRef](#)]
19. Khraisheh, M.; Wu, L.; Al-Muhtaseb, A.H.; Al-Ghouti, M.A. Photocatalytic Disinfection of Escherichia Coli Using TiO<sub>2</sub> P25 and Cu-Doped TiO<sub>2</sub>. *J. Ind. Eng. Chem.* **2015**, *28*, 369–376. [[CrossRef](#)]
20. Carvalho, H.W.P.; Batista, A.P.L.; Hammer, P.; Ramalho, T.C. Photocatalytic Degradation of Methylene Blue by TiO<sub>2</sub>-Cu Thin Films: Theoretical and Experimental Study. *J. Hazard. Mater.* **2010**, *184*, 273–280. [[CrossRef](#)]
21. Zong, M.; Bai, L.; Liu, Y.; Wang, X.; Zhang, X.; Huang, X.; Hang, R.; Tang, B. Antibacterial Ability and Angiogenic Activity of Cu-Ti-O Nanotube Arrays. *Mater. Sci. Eng. C* **2017**, *71*, 93–99. [[CrossRef](#)] [[PubMed](#)]
22. Tryba, B.; Rychtowski, P.; Markowska-Szczupak, A.; Przepiórski, J. Photocatalytic Decomposition of Acetaldehyde on Different TiO<sub>2</sub>-Based Materials: A Review. *Catalysts* **2020**, *10*, 1464. [[CrossRef](#)]
23. Topalian, Z.; Niklasson, G.A.; Granqvist, C.G.; Österlund, L. Spectroscopic Study of the Photofixation of SO<sub>2</sub> on Anatase TiO<sub>2</sub> Thin Films and Their Oleophobic Properties. *ACS Appl. Mater. Interfaces* **2012**, *4*, 672–679. [[CrossRef](#)] [[PubMed](#)]
24. Kumar, C.P.; Gopal, N.O.; Wang, T.C.; Wong, M.-S.; Ke, S.C. EPR Investigation of TiO<sub>2</sub> Nanoparticles with Temperature-Dependent Properties. *J. Phys. Chem. B* **2006**, *110*, 5223–5229. [[CrossRef](#)] [[PubMed](#)]

25. Howe, R.F.; Gratzel, M. EPR Observation of Trapped Electrons in Colloidal Titanium Dioxide. *J. Phys. Chem.* **1985**, *89*, 4495–4499. [[CrossRef](#)]
26. Amano, F. Hydrogen Reduced Rutile Titanium Dioxide Photocatalyst. In *Titanium Dioxide*; Janus, M., Ed.; InTech: Rijeka, Croatia, 2017; ISBN 978-953-51-3413-8.
27. Siriwardane, R.V.; Poston, J.A. Interaction of H<sub>2</sub>S with Zinc Titanate in the Presence of H<sub>2</sub> and CO. *Appl. Surf. Sci.* **1990**, *45*, 131–139. [[CrossRef](#)]
28. Liu, X.; Li, Y.; Peng, S.; Lu, G.; Li, S. Modification of TiO<sub>2</sub> with Sulfate and Phosphate for Enhanced Eosin Y-Sensitized Hydrogen Evolution under Visible Light Illumination. *Photochem. Photobiol. Sci.* **2013**, *12*, 1903–1910. [[CrossRef](#)]
29. Song, X.; Wang, Y.; Song, D.; An, C.; Wang, J. Catalysis of a Nanometre Solid Super Acid of SO<sub>4</sub><sup>2-</sup>/TiO<sub>2</sub> on the Thermal Decomposition of Ammonium Nitrate. *Nanomater. Nanotechnol.* **2016**, *6*, 23. [[CrossRef](#)]
30. Khan, M.E.; Khan, M.M.; Min, B.-K.; Cho, M.H. Microbial Fuel Cell Assisted Band Gap Narrowed TiO<sub>2</sub> for Visible Light-Induced Photocatalytic Activities and Power Generation. *Sci. Rep.* **2018**, *8*, 1723. [[CrossRef](#)]
31. Zhao, Z.; Tan, H.; Zhao, H.; Lv, Y.; Zhou, L.-J.; Song, Y.; Sun, Z. Reduced TiO<sub>2</sub> Rutile Nanorods with Well-Defined Facets and Their Visible-Light Photocatalytic Activity. *Chem. Commun.* **2014**, *50*, 2755–2757. [[CrossRef](#)]
32. Pitchaimuthu, S.; Honda, K.; Suzuki, S.; Naito, A.; Suzuki, N.; Katsumata, K.; Nakata, K.; Ishida, N.; Kitamura, N.; Idemoto, Y.; et al. Solution Plasma Process-Derived Defect-Induced Heterophase Anatase/Brookite TiO<sub>2</sub> Nanocrystals for Enhanced Gaseous Photocatalytic Performance. *ACS Omega* **2018**, *3*, 898–905. [[CrossRef](#)] [[PubMed](#)]
33. Luciu, I.; Bartali, R.; Laidani, N. Influence of Hydrogen Addition to an Ar Plasma on the Structural Properties of TiO<sub>2-x</sub> Thin Films Deposited by RF Sputtering. *J. Phys. D Appl. Phys.* **2012**, *45*, 345302. [[CrossRef](#)]
34. Tryba, B.; Wozniak, M.; Zolnierkiewicz, G.; Guskos, N.; Morawski, A.; Colbeau-Justin, C.; Wrobel, R.; Nitta, A.; Ohtani, B. Influence of an Electronic Structure of N-TiO<sub>2</sub> on Its Photocatalytic Activity towards Decomposition of Acetaldehyde under UV and Fluorescent Lamps Irradiation. *Catalysts* **2018**, *8*, 85. [[CrossRef](#)]
35. Marugán, J.; van Grieken, R.; Sordo, C.; Cruz, C. Kinetics of the Photocatalytic Disinfection of Escherichia Coli Suspensions. *Appl. Catal. B Environ.* **2008**, *82*, 27–36. [[CrossRef](#)]
36. Oh, J.K.; Yegin, Y.; Yang, F.; Zhang, M.; Li, J.; Huang, S.; Verkhoturov, S.V.; Schweikert, E.A.; Perez-Lewis, K.; Scholar, E.A.; et al. The Influence of Surface Chemistry on the Kinetics and Thermodynamics of Bacterial Adhesion. *Sci. Rep.* **2018**, *8*, 17247. [[CrossRef](#)] [[PubMed](#)]
37. Emara, M.M.; Ali, S.H.; Hassan, A.A.; Kassem, T.S.E.; Van Patten, P.G. How Does Photocatalytic Activity Depend on Adsorption, Composition, and Other Key Factors in Mixed Metal Oxide Nanocomposites? *Colloid Interface Sci. Commun.* **2021**, *40*, 100341. [[CrossRef](#)]
38. Wanag, A.; Rokicka, P.; Kusiak-Nejman, E.; Kapica-Kozar, J.; Wrobel, R.J.; Markowska-Szczupak, A.; Morawski, A.W. Antibacterial Properties of TiO<sub>2</sub> Modified with Reduced Graphene Oxide. *Ecotoxicol. Environ. Saf.* **2018**, *147*, 788–793. [[CrossRef](#)]
39. Wyness, A.J.; Paterson, D.M.; Defew, E.C.; Stutter, M.I.; Avery, L.M. The Role of Zeta Potential in the Adhesion of *E. Coli* to Suspended Intertidal Sediments. *Water Res.* **2018**, *142*, 159–166. [[CrossRef](#)]
40. Hu, C.; Guo, J.; Qu, J.; Hu, X. Photocatalytic Degradation of Pathogenic Bacteria with AgI/TiO<sub>2</sub> under Visible Light Irradiation. *Langmuir* **2007**, *23*, 4982–4987. [[CrossRef](#)]